Applied Biological Research 23(2): 196-208; (2021)
DOI: 10.5958/0974-4517.2021.00026.4

BIOPHYSICAL, BIOCHEMICAL AND MICROSCOPIC STUDIES ON WHOLE HISTONE GLYCATED BY DEOXYRIBOSE

Shireen Naaz Islam, Zarina Arif, Moinuddin, Asim Badar and Khursheed Alam*

Department of Biochemistry, Jawaharlal Nehru Medical College, Faculty of Medicine, Aligarh Muslim University, Aligarh-202 002, Uttar Pradesh (India)
*e-mail: *kalam786@rediffmail.com*

(Received 15 January, 2021; accepted 14 March, 2021)

ABSTRACT

Histones, upon reaction with reducing sugars, are known to generate highly reactive advanced glycation end products (AGEs). In this study, we investigated the structural changes associated with the glycation of whole histone by 2-deoxy D-ribose. The deoxy pentose was incubated with whole histone for 12 days and the resultant biophysical and structural changes in the deoxyribose modified-whole histone were investigated thoroughly using biochemical assays, various spectroscopic techniques like UV-visible, fluorescence, FT-IR, and CD, UPLC-MS, and transmission electron microscopy. We found that deoxyribosylation of whole histone formed pentosidine and Nε-carboxymethyl-L-lysine AGEs and was accompanied by an increase in oxidative stress. The histone-AGEs caused gross structural changes in the protein and formed large amorphous aggregates. The presence of such AGE aggregates is likely to interfere with the proper functioning of histones and chromatin, besides exhibiting immunogenicity and generation of autoantibodies against nuclear antigens.

Keywords: 2-Deoxy-D-ribose, histones, mass spectrometry, Nε-carboxymethyl-L-lysine, pentosidine, transmission electron microscopy

INTRODUCTION

2'-Deoxy-D-ribose (dRib), as a part of DNA, is one of the most abundant reducing sugars in living organisms. Moreover, the degradation of thymidine via thymidine phosphorylase is a major source of cellular dRib (Rafi *et al*., 2020). Deoxyribose synthesis in animal tissues may also result from the condensation of glyceraldehyde phosphate with acetaldehyde (McGeown and Malpress, 1952). dRib shows high reactivity towards proteins, even higher than that of D-glucose and D-fructose (Monnier, 1990), leading to the production of glycation intermediates, reactive carbonyl species and AGEs. The deleterious effects of dRib-AGEs have been well-documented. dRib may damage pancreatic β-cells both by oxidative stress and protein glycation (Koh *et al*., 2010; Suh *et al*., 2012). Furthermore, dRib induces oxidative stress and apoptosis in β-cell lines within 24 h (Koh *et al*., 2005).

The long half-life and the presence of a lysine/arginine-rich nucleophilic tail in histones may be favourable to glycation reactions. Zheng *et al*. (2019) observed the accumulation of glycation

---

This research paper is a part of Ph. D thesis to be submitted to Aligarh Muslim University, Aligarh (India)

products specifically on histones in cancer cells, but not in normal cell culture. Functionally, histones regulate a wide range of molecular processes like gene expression and DNA replication and repair (Wolffe, 1998). Any structural modification in histones may affect its DNA binding properties (Ashraf *et al*., 2015). Histone glycosylation can alter its transcriptional program and disrupt the chromatin structure and function thereby contribute to the genomic instability and disease progression (Zheng *et al*., 2019). Other studies propose that hypo-immunity seen in diseases like diabetes mellitus is due to the long term epigenetic impacts of histone glycosylation on immune responses (Zheng *et al*., 2020; Mir *et al*., 2021). Studies have also indicated the vulnerability of histones towards AGE-formation. Gugliucci (1994) demonstrated *in vitro* that rat liver histones can form AGEs in a time- and sugar concentration-dependent manner. Histones-AGEs have also been reported in the liver of diabetic rats and patients, indicating their likely rolein the pathogenesis and/or progression of the disease (Gugliucci and Bendayan, 1995; Jobst and Lakatos, 1996). The lysine residues of H1 and H2B have been reported to be glycoxidatively modified *in vitro* (Liebich *et al*., 1993; Guedes *et al*., 2011). Talasz *et al*. (2002) have reported that core histones are more prone to glycation than the linker histone H1, especially when they are not in the nucleosomal conformation. Further, they documented the formation of cross-links showing disappearance of individual histone molecules and the appearance of dimers and polymers when total histones were glycated non-enzymatically. In spite of the fact that the occurrence and effects of histones-AGEs have been well-described, their structural details are still poorly documented mainly due to their chemical complexity and dynamic nature. In the current study, we examined the effect of dRib glycosylation on the structural properties of whole histone using biochemical assays and biophysical techniques as well as electron microscopy.

MATERIALS AND METHODS

Preparation of whole histone solution

Unfractionated calf thymus whole histone was obtained from Sigma-Aldrich Company (St. Louis, MI, USA; Cat. No. H9250) and dissolved in sterile 10 mM phosphate-buffered saline (PBS), pH 7.4.

Deoxyribosylation of whole histone

All test tubes, reagent bottles, and micropipette tips were autoclaved prior to the use. Whole histone (1 mg mL^{-1}) was mixed with 10, 30 and 50 mM D-deoxyribose dissolved in 10 mM PBS (pH 7.4) and incubated at 37°C for 12 days. A bacteriostatic agent sodium azide (0.02%) was added to all reaction tubes to ensure sterility. At the end of incubation, the preparations were extensively dialyzed against 10 mM PBS. The native whole histone (NWH; 1 $mgmL^{-1}$) and deoxyribosylated-whole histone (dRSWH10, 30 and 50) samples were then stored in aliquots at -20°C for further experiments.

Absorption spectroscopy

The absorption spectra of the native whole histone (NWH) and deoxyribosylated-whole histone (dRSWH) samples were recorded in the wavelength range of 250-450 nm using a spectrophotometer (model UV-1700; Shimadzu Corporation, Japan). Increase in absorbance (hyperchromicity) at 280 nm was calculated from the following equation:

$$\%\ \text{hyperchromicity at 280 nm} = \left(\frac{OD_{dRSWH} - OD_{NWH}}{OD_{dRSWH}}\right) \times 100$$

Detection of Amadori-histone

Native and deoxyribosylated-whole histone samples were subjected to nitroblue tetrazolium (NBT) assay (Johnson *et al*., 1983) for the detection of Amadori products. Briefly, the samples were mixed

with NBT solution (250 µM NBT in 0.1 M carbonate buffer) in a ratio of 1:1 by volume and incubated at 37°C for 2 h. Next, the absorbances of samples were recorded at 550 nm. The concentration of Amadori-histone (in n moles mL^{-1}) was determined using the molar extinction coefficient value of monoformazan (12,640 $cm^{-1} M^{-1}$).

Fluorescence spectroscopy

Fluorescence spectroscopy is a rapid and cost effective technique for the detection of AGEs, since most AGEs have a characteristic fluorescence with λ_{ex} at 370 nm and λ_{em} at around 445 nm (Zaman *et al.*, 2017). For detection of fluorescent AGEs, the NWH and dRSWH samples were excited at 370 nm and emission intensity was recorded in the wavelength range of 380-500 nm on a spectrofluorometer (model RF-5301, Shimadzu Corporation, Japan). Similarly, for detection of pentosidine, a fluorescent AGE with a $\lambda_{ex}/\lambda_{em}$ of 335/390 nm, the samples were excited at 335 nm and the emission spectrum was recorded in the wavelength range of 340-450 nm (Uchiyama *et al.*, 1991). The increase in fluorescence intensity (FI) was calculated using the following equation:

$$\% \text{ increase in FI} = \frac{FI_{dRSWH} - FI_{NWH}}{FI_{dRSWH}} \times 100$$

Determination of free ε-amino group content of dRSWH

The free ε-amino groups of NWH and dRSWH were determined with trinitrobenzene sulfonic acid (TNBS) reagent (Haynes *et al*., 1967). Briefly, a 0.01% (v/v) solution of TNBS was prepared in 0.1 M sodium bicarbonate, following which 500 µL of the sample was mixed with 250 µL of the TNBS solution and incubated at 37°C for 2 h. The reaction was stopped with 250 µL of 10% SDS and 125 µL of 1 N HCl and the absorbance was recorded at 335 nm.

Determination of free arginine residues of dRSWH

The arginine content of NWH and dRSWH samples was estimated by a modified Sakaguchi method (Sakaguchi, 1950). Briefly, 1 mL of protein sample was treated with a few drops each of 10% NaOH and 0.04% α-naphthol (dissolved in ethanol) and 1 mL 0.06 N sodium hypochlorite. The appearance of a pink color indicated the presence of arginine in samples. The absorbance was read at 500 nm.

Estimation of carbonyl content

Carbonyl content of NWH and dRSWH samples was estimated by dinitrophenyl hydrazine (DNPH) assay using an established protocol (Levine *et al*., 1990). The carbonyl concentration in the samples was calculated using the molar extinction coefficient of DNPH (22,000 $M^{-1} cm^{-1}$).

Estimation of thiol content

Free sulfhydryl groups (thiol) of NWH and dRSWH samples were estimated by a colorimetric assay utilizing DTNB (Ellman's reagent) (Ellman, 1959). Sodium acetate (50 mM) and 2 mM DTNB solutions were prepared in distilled water. The NWH and dRSWH samples (150 µL) were mixed with 3 mL DTNB solution and incubated in dark at room temperature for 30 min. The absorbance was then read at 412 nm and the thiol content calculated by using the molar extinction coefficient of DTNB (0.01415 $\mu M^{-1} cm^{-1}$).

Detection of Nε-carboxymethyl lysine (CML) by UPLC-MS

Acid hydrolysates of NWH and dRSWH, along with commercially obtained CML standard (IRIS Biotech GMBH, Germany), were processed on UPLC-MS machine. The peaks observed for the NWH and dRSWH samples were compared with the peak of standard CML. Acid hydrolysates of NWH and dRSWH were prepared by incubating the protein samples with 6 mol L^{-1} HCl at 95°C for 18 h and then filtered through a 0.24 µm filter. Acetonitrile was used as solvent and a flow rate of 0.8 mL min^{-1} was maintained through an X-Bridge C-18 column (2.5 x 100 mm; 1.7 µm particle size). Mass spectrometric analysis was carried out on an Acquity UPLC-MS system (Waters, MA,

USA) operated in positive ion mode. Previous studies have verified the presence of non-fluorescent AGEs like CML and CEL in samples by LC-MS analysis in a similar manner (Naila *et al.*, 2004).

FT-IR spectroscopy

FT-IR is a rapid and nondestructive technique widely used to determine the secondary structure and local conformational changes in proteins. To elucidate the changes in the secondary structure of dRSWH, FT-IR spectroscopy was carried out using Perkin-Elmer FT-IR spectrophotometer. Infrared spectral readings were recorded between 1400-1800 cm^{-1}, which covers both amide I and II bands.

Circular dichroism (CD) measurements

The CD spectrum in the far UV region corresponds to peptide bond absorption. The technique is used to determine regular secondary structural features such as α-helix and β-sheet. Far-UV CD profiles of NWH and dRSWH samples were recorded using a spectropolarimeter calibrated with D-10-camphor-sulfonic acid. Cuvette of 1 mm path length was used for obtaining spectra in the wavelength range of 190-260 nm at a scan speed of 100 nm min^{-1} and response time of 1 s (Kelly and Price, 1997).

Dynamic light scattering (DLS) studies

Dynamic light scattering technique is routinely used to determine the hydrodynamic diameter and the size of protein molecules. Therefore, the NWH and dRSWH were subjected to DLS analysis using DynaPro-TC-04 DLS equipment (Wyatt Technology, CA, USA). Briefly, the samples were spun at 10,000 rpm for 10 min and passed through a microfilter into a 12 µL quartz cuvette. Data analysis was done using Dynamics 6.10.0.10 software (Arfat *et al.*, 2014). The mean hydrodynamic diameter (D_h) of the molecules was calculated with the help of the Stokes-Einstein equation given below:

$$D_h = \frac{2kT}{6\pi\eta D_w^{25^0C}}$$

Where, D_h is the hydrodynamic diameter, k is the Boltzmann's constant, T is the absolute temperature, η is the viscosity of water and $D_w^{25^0C}$ is translational diffusion coefficient of water at 25°C.

TEM imaging of NWH and dRSWH

Two dimensional images of individual macromolecular complexes of NWH and dRSWH samples were obtained by using JEOL transmission electron microscope (Tokyo, Japan) operated at an accelerating voltage of 180 kV. The samples were fixed, dehydrated using ethanol, and passed through propylene dioxide. Formvar film was used for coating the samples once the grids were prepared and images were viewed using iTEM and TIA software.

Statistical analysis

All tests were carried out in duplicate and the results are expressed as mean ± SD. The statistical significance of the values was calculated using one-way ANOVA and Dunnett's test and a p-value of < 0.05 was considered significant.

RESULTS AND DISCUSSION

The persistence of apoptotic debris due to poor or delayed clearance is a likely source of auto-antigen(s) in autoimmune diseases (Szondy *et al.*, 2014). Studies have shown that apoptosis induces the release of individual nucleosomal histones (Wu *et al.*, 2002) and they may be glycosylated by the circulating carbohydrates. Glycation studies conducted on various histone variants have shown their involvement in the development and progression of chronic inflammatory diseases (Khan *et*

al., 2009; Ashraf *et al*., 2015), but the effects of such glycation reactions on the structure, conformation, mass, and morphologyof the whole histone have not been documented in detail.

Native whole histone dissolved in PBS, pH 7.4 showed maximum absorbance at 280 nm (Fig. 1). However, modification with 10, 30 and 50 mM deoxyribose resulted in 55.6, 74.8 and 79.4% hyperchromicity, respectively, as compared to NWH. The hyperchromicities observed in dRSWH samples at 280 nm indicated perturbate in protein structure.

AGEs formation involve non-enzymatic glycosylation of biological macromolecules wherein carbonyl moieties undergo covalent attachment with the amino groups of proteins, lipids and nucleic acids and form unstable Schiff base or aldimines (Dyer *et al*., 1991; Singh *et al*., 2001). The aldimines undergo Amadori rearrangement forming stable fructosamine derivatives which progressively undergo complex chemical rearrangements and reactions to generate irreversible AGEs (Hodge, 1953; Arena *et al*., 2014). NBT is a yellow-coloured dye which is reduced by Amadori adducts (fructosamine) and forms purple-coloured monoformazan with λ_{max} at 525 nm. As shown in Fig. 2, fructosamine formation in dRSWH samples was completed on day 4, and the fructosamine content in dRSWH samples was significantly higher than that of NWH ($p < 0.001$). The monoformazan was found to be 27.53, 61.55 and 96.52 n mol mL^{-1} in dRSWH modified with 10, 30 and 50 mM deoxyribose, respectively. In NWH, the monoformazan was found to be 3.25 n mol mL^{-1}. From the day 5 onwards, the fructosamine content started decreasing and eventually plateaued, suggesting a gradual conversion of Amadori adducts into AGEs (Singh *et al*., 2001).

Fig. 3 shows the emission spectra of NWH and dRSWH samples. dRSWH samples excited at 370 nm showed peaks at around 445 nm, indicating the presence of fluorescent AGEs in the samples (Zaman *et al*., 2018). Till date, more than 20 AGE structures have been identified and most of them are intrinsically fluorescent. How-

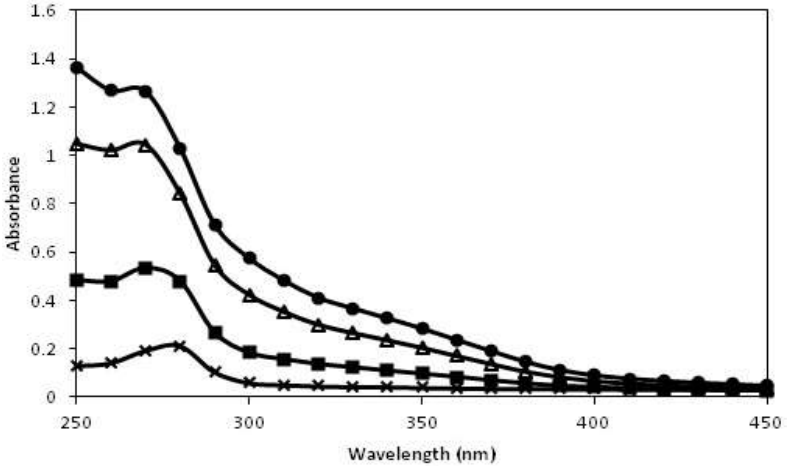

Fig. 1: UV-visible spectra of NWH (-x-) and dRSWH modified with 10 (-■-), 30 (-Δ-), and 50 mM (-●-) deoxyribose

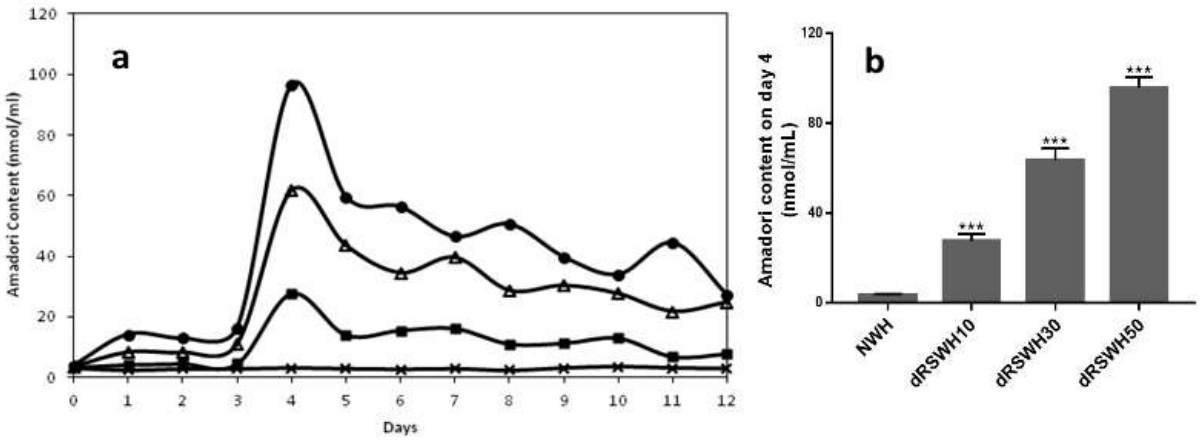

Fig. 2: a) Effect of time on the level of Amadori adducts in NWH (-x-) and dRSWH at deoxyribose concentrations of 10 (-■-), 30 (-Δ-), and 50 mM (-●-); b) Amadori content detected in the dRSWH samples on day 4 compared to NWH. ***$p < 0.001$

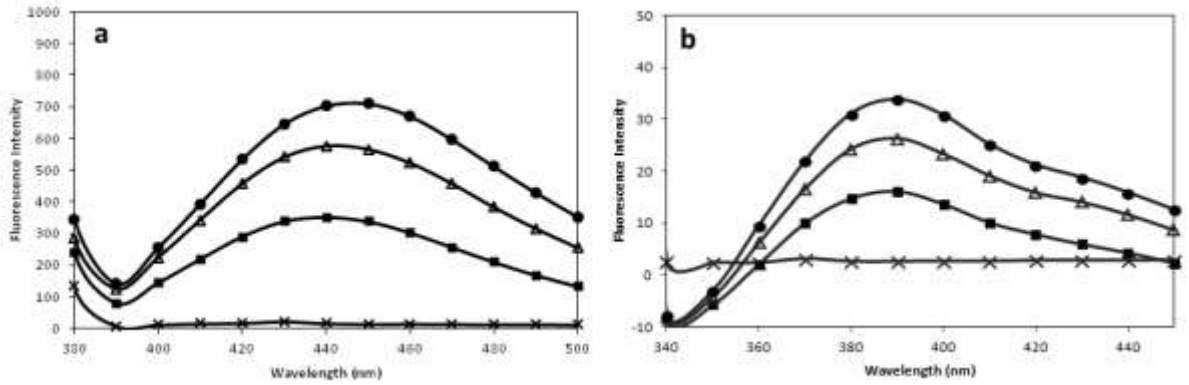

Fig. 3:The emission spectra of NWH (-x-) and dRSWH incubated for 12 days with 10 (-■-), 30 (-Δ-) and 50 mM (-●-)deoxyribose when all samples were excited at (a) 370 nm, and (b) 335 nm

ever, due to their complex and heterogenous nature only some of these structures have been well defined. A well-characterized fluorescent AGE is the pentosidine, an arginine-lysine cross-link compound (Vetter, 2015). Subsequent analysis carried out at λ_{ex} of 335 nm showed peaks at around 390 nm, suggesting the presence of pentosidine in dRSWHsamples but not in NWH [Fig. 3b] (Uchiyama *et al*., 1991).

The lysine and arginine content of NWH and dRSWH samples were then estimated by trinitrobenzene sulfonic acid reagent and Sakaguchi reaction, respectively. The amounts of lysine/ arginine in NWH were considered to be 100% and the percentages of lysine/arginine in three versions of dRSWH were calculated relative to that in NWH. The decrease in the content of free lysine and arginine residues between the native and deoxyribosylated WH samples was highly significant ($p < 0.001$ in each case) [Fig. 4a]. This clearly suggests the formation of AGEs, since the nucleophilic lysine and/or arginine residues are the primary sites of glycosylation in proteins (Thorpe and Baynes, 2003). The reactivity of lysine was greater than that of arginine. This may be explained by the fact that amino groups with lower pKa values are observed to be more reactive in glycosylation reactions (pKa of lysine and arginine are 10.5 and 12.5, respectively) (Bunn *et al*., 1979).

Since glycosylation reactions are accompanied by an increase in the reactive oxygen species (Khan *et al*., 2017), we evaluated the oxidative stress in NWH and dRSWH by two reliable assays: Ellman's test for free sulfhydryl and DNPH assay for carbonyl (Shacter, 2000). As shown in Fig. 4b, the carbonyl content increased from 6.89 in NWH to 33.1, 47.4, and 55.32 nmol mg^{-1} in the dRSWH samples modified by 10, 30 and 50 mM deoxyribose, respectively. On the other hand, the thiol

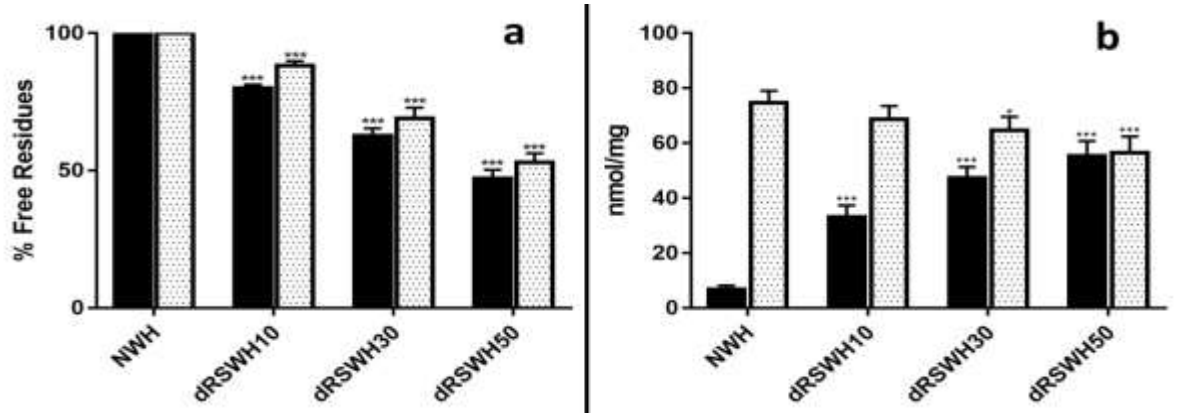

Fig. 4: a) Percentages of free lysine (▉) and arginine (▒) residues in dRSWH at 10, 30 and 50 mM deoxyribose, relative to that in NWH. b) Amount of carbonyl (▉) and thiol (▒) in NWH and dRSWH10, 30 and 50 samples. Significant differences are reported as * (p = 0.05) or * (p < 0.001) as compared to NWH**

(sulfhydryl) content decreased from 74.7 n mol mg^{-1} in NWH to 68.65, 64.6 and 56.5 n mol mg^{-1} in dRSWH 10, 30 and 50, respectively**.** The formation of more and more protein carbonyls may be attributed to the oxidation of amino acids or to the oxidative cleavage of protein backbone. In addition, glycosylation reactions are known to produce reactive carbonyl derivatives capable of reacting with proteins (Levine *et al.*, 1994). Similarly, the estimation of the free thiol (-SH) in proteins is also a measure of the oxidative stress on proteins. The oxidation of thiol-containing residues, such as cysteine, changes the oxidation state of sulfur, rather than that of the carbon. This leads to the formation of a disulfide (-S-S-) bridge between the two residues, thus decreasing the total thiol content of the protein (Ellman, 1959). The decrease in free thiol accompanied by increase in carbonyl clearly suggested imbalance in the redox state and AGEs formation. Confirmation of AGEs formation was provided by the presence of CML, an authentic marker of non-fluorescent AGEs (Ikeda *et al.*, 1996), in dRSWH samples. Nε-(1-carboxymethyl)-L-lysine (CML) is a non-crosslinked and non-fluorescent AGE produced by oxidative modification of glycated proteins under oxidative stress (Ahmed *et al.*, 1997). The UPLC chromatogram of the commercially available CML and that of dRSWH modified by 50 mM deoxyribose showed peaks at retention times of 2.15 and 2.16 min [Fig. 5(i) a and c], respectively. The hydrolyzed NWH processed under identical conditions did not exhibit CML peak [Fig. 5(i) b]. Additionally, the mass spectra of CML fraction showed a base peak of high intensity at an m/z value of 205.12, and a product ion peak at 131.49 m/z [Fig. 5(ii) a], which correlates with the reported molecular mass of standard CML (204.22 g mol^{-1}). In case of NWH, no peak exhibited similiarity with that of CML standard [Fig. 5(ii)b], while that of hydrolyzed dRSWH showed distinct peaks at m/z values of 205.7 and 131.81 [Fig. 5(ii) c], indicating the presence of CML.

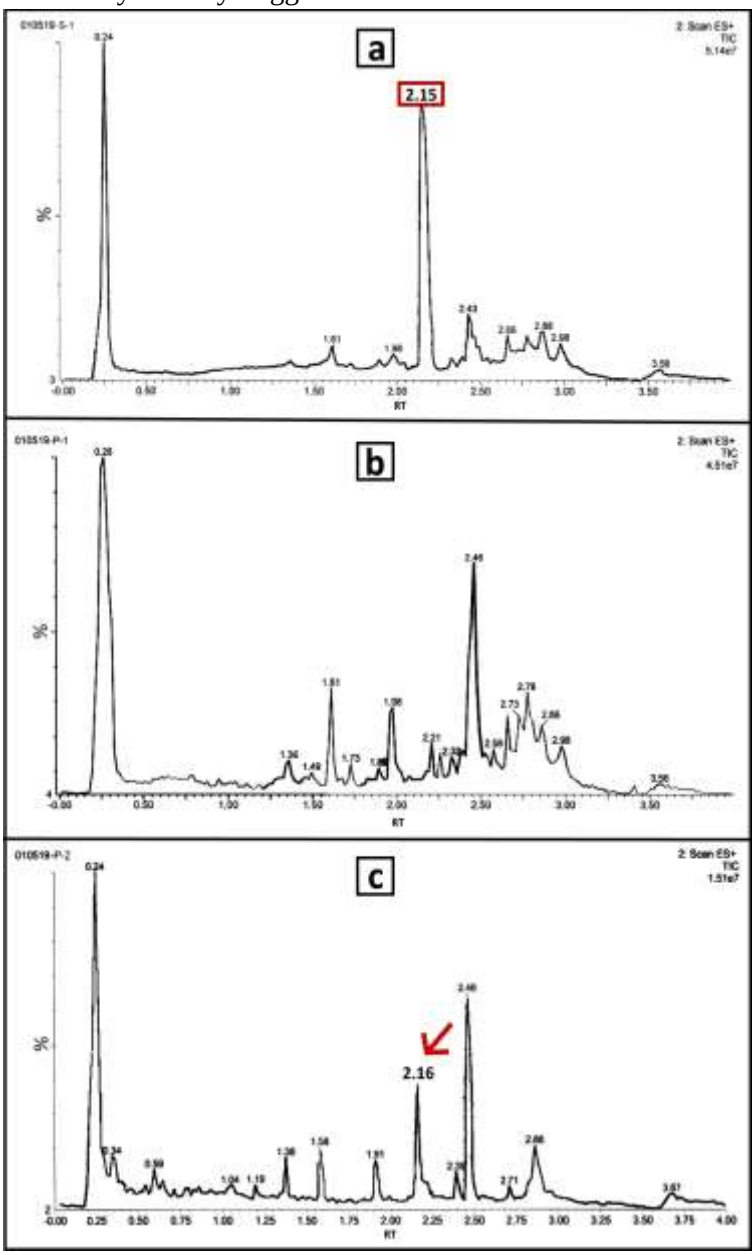

Fig. 5(i) UPLC chromatogram of (a) commercially obtained CML, (b) hydrolyzed NWH, and (c) hydrolyzed dRSWH modified with 50 mM deoxyribose.

The effect of deoxy-ribosylation on the secondary structure of dRSWH was analyzed by FT-IR and far UV-CD spectroscopic techniques.

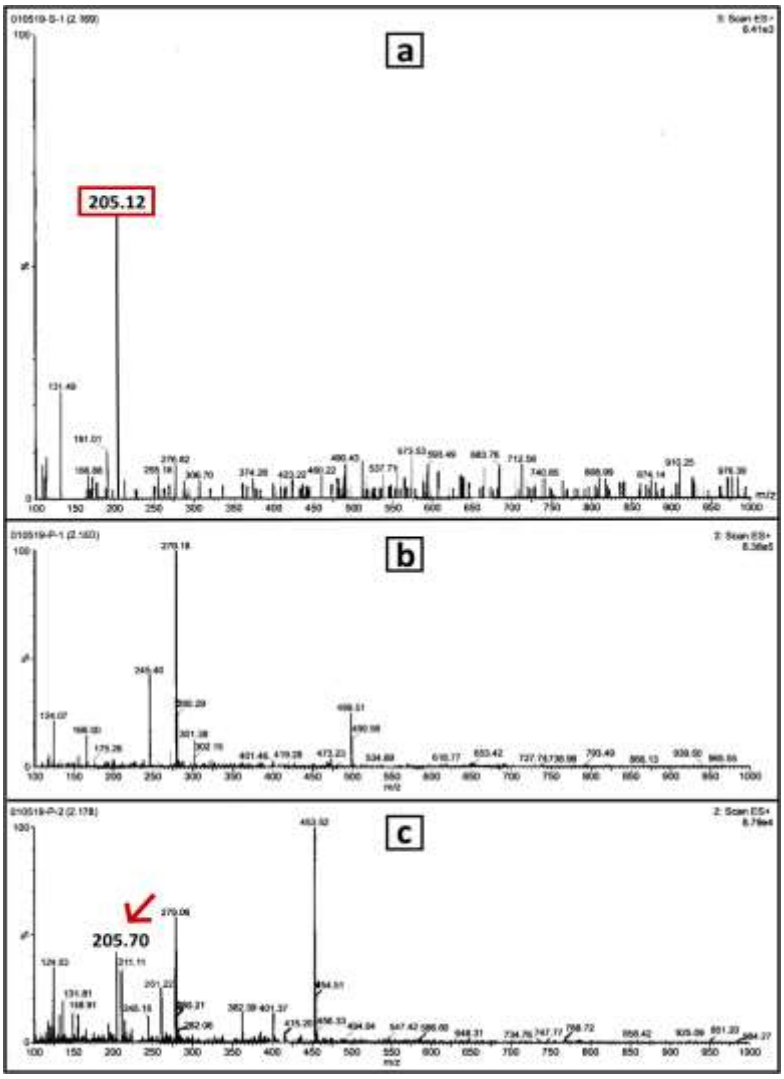

Fig. 5(ii) UPLC-MS profile of (a) commercially available CML, (b) hydrolyzed NWH, and (c) hydrolyzed dRSWH modified with 50 mM deoxyribose

The FTIR-ATR spectra collected in the range of 1500-1800 cm^{-1} showed two bands: an amide I band (1600-1700 cm^{-1}) arising due to C=O stretching, and an amide II band (1500-1600 cm^{-1}) which arises due to the C-N stretching coupled with N-H bending vibrations (Liu *et al*., 2003; Ashraf *et al*., 2014). The intensities of peaks corresponding to the three versions of dRSWH showed a large decrease in band intensities as compared to that of NWH (Fig. 6a). Further, the shifts in amide I and amide II band positions were observed for deoxyribosylated-WH samples (Table 1). These shift in band positions may be attributed to perturbations in the secondary structure of protein. The CD spectroscopy data of samples further corroborated the results of FTIR spectroscopy. The NWH showed two ellipticity peaks- one at 222 nm (-17.23 mdeg), and another at 208 nm (-28.94 mdeg) [Fig. 6b; Table 1].

After modification with deoxyribose, the samples exhibited a loss in negative ellipticity at 222 and 208 nm, suggesting a decrease in α-helical content (Corbin *et al*., 1998). Meanwhile, the absence of a peak at around 215-218 nm indicated that the deoxyribosylation of whole histones is not accompanied by any increase in β-sheet. Previous studies on glycation of proteins have reported the formation of ordered amyloid AGE aggregates (Khan *et al*., 2017; Zaman *et al*., 2018) which is facilitated by an increase in β-sheet conformation (Von Bergen *et al*., 2005).

Our results indicated that deoxyribosylation of whole histones is probably accompanied by the formation of disordered amorphous aggregates rather than ordered amyloid aggregates. To confirm

Table 1: Summary of some biophysical characteristics of NWH and dRSWH

		NWH	dRSWH10	dRSWH30	dRSWH50
Amide I (cm^{-1})		1662	1653	1644	1638
Amide II (cm^{-1})		1548	1548	1547	1544
Ellipticity (mdeg)	208 nm	-28.94	-26.35	-22.70	-19.16
	222 nm	-17.23	-14.89	-13.04	-12.16
Hydrodynamic diameter (D_h)		~58.8	~91.3	~122	~190

confirm this, the dRSWH-AGEs were analyzed by DLS and TEM. The hydrodynamic diameter (D_h) of NWH was found to be 58.8 nm (Fig. 7a), while those of dRSWH modified by 10, 30 and 50 mM deoxyribose were found to be approximately 91.3, 122 and 190 nm, respectively (Fig. 7b-d; Table 1). Previous studies have reported the formation of large histone polymers as a result of random aggregation (Toennies and Bakay, 1955; Van Holde and Isenberg, 1975), which were distinct from the nucleosomal histone dimerization and tetramerization. Cruft *et al*. (1958) reported that even the smallest of such aggregates are 9-10 folds larger than the unaggregated histone. A similar explanation may be offered to the unexpectedly large hydrodynamic diameter (D_h) observed

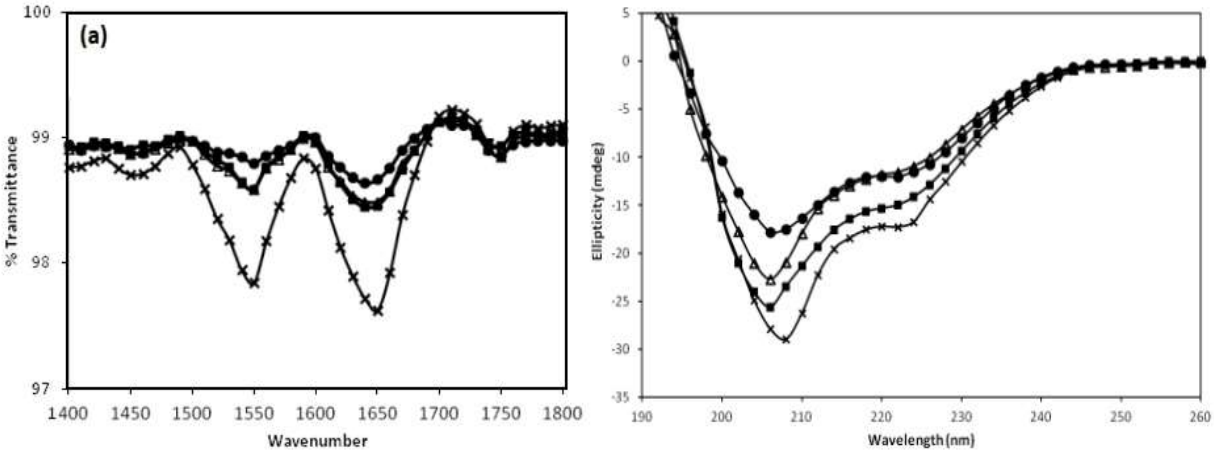

Fig. 6: (a) FT-IR spectra depicting Amide I and II bands, and (b) far-UV CD spectra of NWH (-x-) and dRSWH modified with deoxyribose: 10 mM (-■-), 30 mM (-Δ-), and 50 mM (-●-).

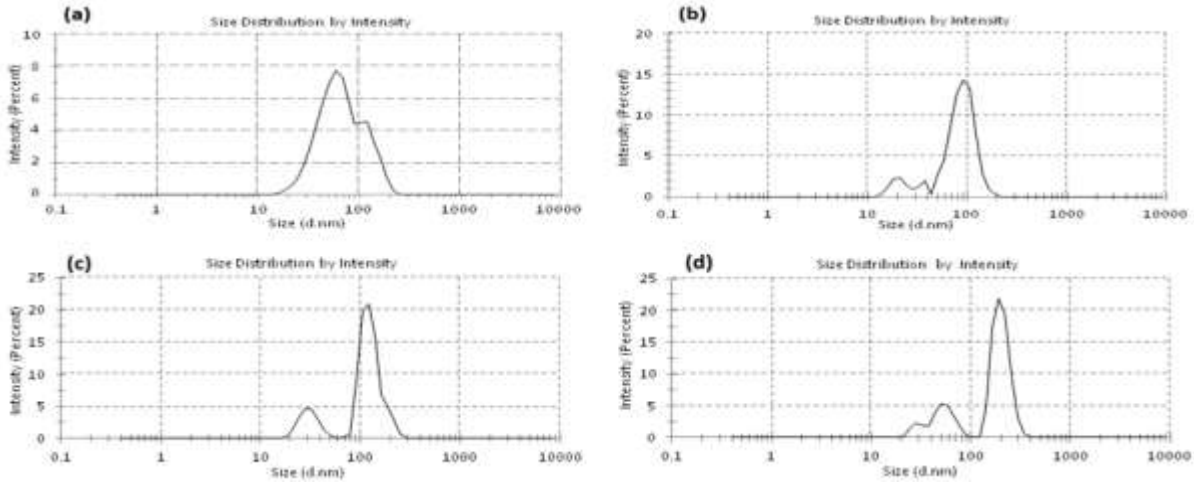

Fig. 7: Dynamic light scattering profiles of (a) NWH, (b) dRSWH modified with 10 mM deoxyribose, (c) dRSWH modified with 30 mM deoxyribose, and (d) dRSWH modified with 50 mM deoxyribose

by us for NWH. This was further supported by the TEM micrographs, which depicted aggregation in the NWH sample (Fig. 8a). Allgen (1950) proposed that the aggregation of unfractionated histones may be due to their high charge density and dipole moment. Nevertheless, the reaction of dRib with whole histone, leading to the generation of histone-AGEs was evident from the significantly greater hydrodynamic diameter observed for dRSWH analogues as compared to native WH; this suggests AGE-aggregate formation. This was visually confirmed by subjecting the dRSWH samples to TEM imaging (Fig. 8b and c). The microphotographs revealed the formation of irregular amorphous AGE aggregates, rather than fibrillar amyloid aggregates, as was suggested by

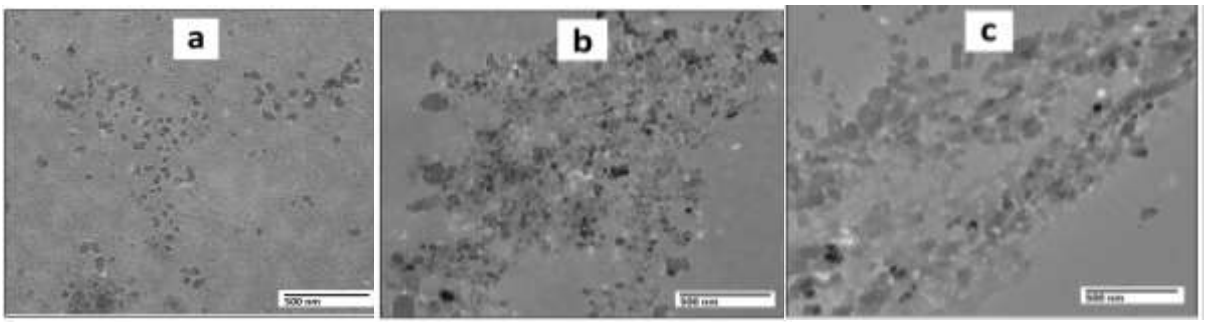

Fig. 8: TEM microphotographs of (a) NWH (b) dRSWH modified with 30 mM deoxyribose, and (c) dRSWH modified with 50 mM deoxyribose.

the far-UV CD results. While the exact kinetics are not yet well elucidated, the exposed hydrophobic surfaces of unfolded proteins are believed to promote amorphous aggregate formation (Yoshimura *et al.*, 2012). Mir *et al*. (2015a) have reported that amorphous aggregates produced as a result of histone glycation are highly immunogenic and have been implicated in the autoimmune response in cancer (Mir *et al.*, 2015b). Furthermore, protein AGE-aggregates are also known to play a critical role in the pathogenesis of various diseases due to accumulation in organs and/or interaction with cellular components.

Conclusion: The study demonstrated that deoxyribose is a potent glycating agent and can influence the molecular size, secondary structure and redox status of the whole histone; leading to AGEs formation and disordered amorphous aggregates. Further studies may be aimed at investigating the presence and pathogenic role of such histone-AGE aggregates in autoimmune diseases especially those involving nuclear antigens such as SLE.

Acknowledgements: The authors are grateful for the access to the DST-FIST instrument facilities of the Department of Biochemistry, J.N. Medical College, A.M.U., and would also like to acknowledge the Interdisciplinary Biotechnology Unit, A.M.U., and the University Sophisticated Instrument Facility, A.M.U. for their support.

REFERENCES

Ahmed, M.U., Frye, E.B., Degenhardt, T.P., Thorpe, S.R. and Baynes, J.W. 1997. N-epsilon-(carboxyethyl) lysine, a product of the chemical modification of proteins by methylglyoxal, increases with age in human lens proteins. *The Biochemical Journal*, **324:** 565-570.

Allgen, L.G. 1950. A dielectric study of nucleohistone from calf thymus. *Acta Physiologica Scandinavica. Supplementum*, **22:** 1-140.

Arena, S., Salzano, A.M., Renzone, G., D'Ambrosio, C. and Scaloni, A. 2014. Non-enzymatic glycation and glycoxidation protein products in foods and diseases: An interconnected, complex scenario fully open to innovative proteomic studies. *Mass Spectrometry Reviews*, **33**: 49-77.

Arfat, M.Y., Ashraf, J.M., Arif, Z., Moinuddin and Alam, K. 2014. Fine characterization of glucosylated human IgG by biochemical and biophysical methods. *International Journal of Biological Macromolecules*, **69**: 408-415.

Ashraf, J.M., Ahmad, S., Rabbani, G., Jan, A.T., Lee, E.J., Khan, R.H. and Choi, I. 2014. Physicochemical analysis of structural alteration and advanced glycation end products generation during glycation of H2A histone by 3-deoxyglucosone. *IUBMB Life*, **66:** 686-693.

Ashraf, J.M., Rabbani, G., Ahmad, S., Hasan, Q., Khan, R.H., Alam, K. and Choi, I.C. 2015.

Glycation of H1 histone by 3-deoxyglucosone: Effects on protein structure and generation of different advanced glycation end products. *PLoS ONE*, **10: [***DOI:10.1371/journal.pone.0130630*].

Bunn, H.F., Shapiro, R., McManus, M., Garrick, L., McDonald, M.J., Gallop, P.M. and Gabbay, K.H. 1979. Structural heterogeneity of human hemoglobin A due to nonenzymatic glycosylation. *The Journal of Biological Chemistry*, **254:** 3892-3898.

Corbin, J., Méthot, N., Wang, H.H., Baenziger, J.E. and Blanton, M.P. 1998. Secondary structure analysis of individual transmembrane segments of the nicotinic acetylcholine receptor by circular dichroism and Fourier transform infrared spectroscopy. *The Journal of Biological Chemistry*, **273**: 771-777.

Cruft, H.J., Mauritzen, C.M. and Stedman, E. 1958. The isolation of beta-histone from calf thymocytes and the factors affecting its aggregation. *Proceedings of the Royal Society of London. Series B, Containing Papers of a Biological Character. Royal Society (Great Britain)*, **149**: 21-35.

Dyer, D.G., Blackledge, J.A., Thorpe, S.R. and Baynes, J.W. 1991. Formation of pentosidine during nonenzymatic browning of proteins by glucose: Identification of glucose and other carbohydrates as possible precursors of pentosidine *in vivo*. *The Journal of Biological Chemistry*, **266**: 11654-11660.

Ellman, G.L. 1959. Tissue sulfhydryl groups. *Archives of Biochemistry and Biophysics*, **82**: 70-77.

Guedes, S., Vitorino, R., Domingues, M.R.M., Amado, F. and Domingues, P. 2011. Glycation and oxidation of histones H2B and H1: *In vitro* study and characterization by mass spectrometry. *Analytical and Bioanalytical Chemistry*, **399**: 3529-3539.

Gugliucci, A. 1994. Advanced glycation of rat liver histone octamers: An *in vitro* study. *Biochemical and Biophysical Research Communications*, **203**: 588-593.

Gugliucci, A. and Bendayan, M. 1995. Histones from diabetic rats contain increased levels of advanced glycation end products. *Biochemical and Biophysical Research Communications*, **212**: 56-62.

Haynes, R., Osuga, D.T. and Feeney, R.E. 1967. Modification of amino groups in inhibitors of proteolytic enzymes. *Biochemistry*, **6**: 541-547.

Hodge, J.E. 1953. Chemistry of browning reaction in model systems. *Agricultural and Food Chemistry*, **1***:* 928-943.

Ikeda, K., Higashi, T., Sano, H., Jinnouchi, Y., Yoshida, M., Araki, Ueda, S. and Horiuchi, S. 1996. N^{ε} -(carboxymethyl) lysine protein adduct is a major immunological epitope in proteins modified with advanced glycation end products of the maillard reaction. *Biochemistry*, **35:** 8075-8083.

Jobst, K. and Lakatos, A. 1996. The liver cell histones of diabetic patients contain glycation endproducts (AGEs) which may be lipofuscin components. *Clinica Chimica Acta*, **256**: 203-204.

Johnson, R.N., Metcalf, P.A. and Baker, J.R. 1983. Fructosamine: A new approach to the estimation of serum glycosylprotein. An index of diabetic control. *Clinica Chimica Acta*, **127:** 87-95.

Kelly, S.M. and Price, N.C. 1997. The application of circular dichroism to studies of protein folding and unfolding. *Biochimica et Biophysica Acta*, **1338:** 161-185.

Khan, M.A., Dixit, K., Jabeen, S., Moinuddin and Alam, K. 2009. Impact of peroxynitrite modification on structure and immunogenicity of H2A histone. *Scandinavian Journal of Immunology*, **69**: 99-109.

Khan, M.A, Arif, Z., Moinuddin and Alam, K. 2017. Characterization of methylglyoxal-modified human IgG by physicochemical methods. *Journal of Biomolecular Structure and Dynamics*, **1102**: 1-12.

Koh, G., Lee, D.H. and Woo, J.T. 2010. 2-Deoxy-D-ribose induces cellular damage by increasing oxidative stress and protein glycation in a pancreatic beta-cell line. *Metabolism: Clinical and*

Experimental, **59**: 325-332.

Koh, G., Suh, K.S., Chon, S., Oh, S., Woo, J.T., Kim, S.W., Kim, J.W and Kim, Y.S. 2005. Elevated cAMP level attenuates 2-deoxy-d-ribose-induced oxidative damage in pancreatic β-cells. *Archives of Biochemistry and Biophysics*, **438***:* 70-79.

Levine, R.L., Garland, D., Oliver, C.N., Amici, A., Climent, I., Lenz, A.G., Ahn, B.W., Shaltiel, S. and Stdtman, E.R. 1990. Determination of carbonyl content in oxidatively modified proteins. *Methods in Enzymology*, **186**: 464-478.

Levine, R.L., Williams, J.A., Stadtman, E.P. and Shacter, E. 1994. Carbonyl assays for determination of oxidatively modified proteins. *Methods in Enzymology*, **233:** 346-357.

Liebich, H.M., Gesele, E., Wirth, C., Wöl, J., Jobst, K. and Lakatos, A. 1993. Non-enzymatic glycation of histones. *Biological Mass Spectrometry*, **22:** 121-123.

Liu, Y., Xie, M., Kang, J. and Zheng, D. 2003. Studies on the interaction of total saponins of Panax notoginseng and human albumin by Fourier transform infrared spectroscopy. *Spectrochimica Acta. Part A, Molecular and Biomolecular Spectroscopy*, **59**: 2747-2758.

McGeown, M.G. and Malpress, F.H. 1952. Synthesis of deoxyribose in animal tissues. *Nature (London)*, **170:** 575-576.

Mir, A.R., Habib, S. and Moinuddin. 2021. Recent advances in histone glycation: Emerging role in diabetes and cancer. *Glycobiology*, [*DOI: 10.1093/glycob/cwab011*].

Mir, A.R., Moinuddin, Habib, S., Khan, F., Alam, K. and Ali, A. 2015a. Structural changes in histone H2A by methylglyoxal generate highly immunogenic amorphous aggregates with implications in auto-immune response in cancer. *Glycobiology*, **26**: 129-141.

Mir, A.R., Uddin, M., Khan, F., Alam, K. and Ali, A. 2015b. Dicarbonyl induced structural perturbations make histone H1 highly immunogenic and generate an auto-immune response in cancer. *PLoS ONE*, **10**(8): e0136197 [*DOI: 10.1371/journal.pone.0136197*].

Monnier, V.M. 1990. Nonenzymatic glycosylation, the Maillard reaction and the aging process. *Journal of Gerontology*, **45:** B105-111.

Rafi, Z., Alouffi, S., Khan, M.S. and Ahmad, S. 2020. 2'-Deoxyribose mediated glycation leads to alterations in BSA structure via generation of carbonyl species. *Current Protein and Peptide Science*, **21:** 924-935.

Sakaguchi, S. 1950. A new method for the colorimetric determination of arginine. *Journal of Biochemistry*, **37:** 231-236.

Shacter, E. 2000. Quantification and significance of protein oxidation in biological samples. *Drug Metabolism Reviews*, **32**: 307-326.

Singh, R., Barden, A., Mori, T. and Beilin, L. 2001. Advanced glycation end-products: A review. *Diabetologia*, **44:** 129-146.

Suh, K.S., Oh, S., Woo, J.T., Kim, S.W., Kim, J.W., Kim, Y.S. and Chon, S. 2012. Apigenin attenuates 2-deoxy-D-ribose-iInduced oxidative cell damage in HIT-T15 pancreatic β-cells. *Biological and Pharmaceutical Bulletin*, **35:** 121-126.

Szondy, Z., Garabuczi, E., Joós, G., Tsay, G.J. and Sarang, Z. 2014. Impaired clearance of apoptotic cells in chronic inflammatory diseases: Therapeutic implications. *Frontiers in Immunology*, **5:** 354 [*DOI: 10.3389/fimmu.2014.00354*].

Talasz, H., Wasserer, S. and Puschendorf, B. 2002. Nonenzymatic glycation of histones *in vitro* and *in vivo*. *Journal of Cellular Biochemistry*, **85**: 24-34.

Thorpe, S.R. and Baynes, J.W. 2003. Maillard reaction products in tissue proteins: New products and new perspectives. *Amino Acids*, **25**: 275-281.

Toennies, G. and Bakay, B. 1955. Characterization and total recovery of the component proteins of a deoxyribonucleoprotein. *Nature (London)*, **176:** 696-697.

Uchiyama, A., Ohishi, O., Takahashi, M., Kushida, K., Inoue, T., Fujie, M. and Horiuchi, K. 1991. Fluorophores from aging human articular cartilage. *Journal of Biochemistry*, **110:** 714-718.

Van Holde, K.E. and Isenberg, I. 1975. Histone interactions and chromatin structure. *Accounts of Chemical Research*, **254**: 3892-3898.

Vetter, S. W. 2015. Glycated serum albumin and age receptors. *Advances in Clinical Chemistry*, **72:** 205-275.

Von Bergen, M., Barghorn, S., Biernat, J., Mandelkow, E.M. and Mandelkow, E. 2005. Tau aggregation is driven by a transition from random coil to beta sheet structure. *Biochimica et Biophysica Acta - Molecular Basis of Disease*, **1739:** 158-166.

Wolffe, A.P. 1998. Packaging principle: How DNA methylation and histone acetylation control the transcriptional activity of chromatin? *Journal of Experimental Zoology*, **282**, 239-244.

Wu, D., Ingram, A., Lahti, J.H., Mazza, B., Grenet, J., Kapoor, A., Liu, L., Kidd, V.J. and Tang, D. 2002. Apoptotic release of histones from nucleosomes. *The Journal of Biological Chemistry*, **277:** 12001-12008.

Yoshimura, Y., Lin, Y., Yagi, H., Lee, Y.H., Kitayama, H., Sakurai, K., So, M., Ogi, H., Naiki, H. and Goto, Y. 2012. Distinguishing crystal-like amyloid fibrils and glass-like amorphous aggregates from their kinetics of formation. *Proceedings of the National Academy of Sciences of the United States of America*, **109:** 14446-14451.

Zaman, A., Arif, Z. and Alam, K. 2017. Fructosylation induced structural changes in mammalian DNA examined by biophysical techniques. *Spectrochimica Acta - Part A: Molecular and Biomolecular Spectroscopy*, **174**: 171-176.

Zaman, A., Arif, Z., Moinuddin and Alam, K. 2018. Fructose-human serum albumin interaction undergoes numerous biophysical and biochemical changes before forming AGEs and aggregates. *International Journal of Biological Macromolecules*, **109:** 896-906.

Zheng, Q., Maksimovic, I., Upad, A. and David, Y. 2020. Non-enzymatic covalent modifications: a new link between metabolism and epigenetics. *Protein and Cell*, **11:** 401-416.

Zheng, Q., Omans, N.D., Leicher, R., Osunsade, A., Agustinus, A.S., Finkin-Groner, E., D′Ambrosio, H., Liu, B., Chandarlapaty, S., Liu, S. and David, Y. 2019. Reversible histone glycation is associated with disease-related changes in chromatin architecture. *Nature Communications*, **10**(1): 1-12 [*DOI: 10.1038/s41467-019-09192-z*].